

Laser-induced continuum structure and third-harmonic generation in sodium: Theory and calculations

Jian Zhang

Department of Physics, University of Southern California, Los Angeles, California 90089-0484

P. Lambropoulos

Department of Physics, University of Southern California, Los Angeles, California 90089-0484;

Foundation for Research and Technology-Hellas, Institute of Electronic Structure and Laser,

P.O. Box 1527, Heraklion 71110, Crete, Greece;

and Department of Physics, University of Crete, Crete, Greece

(Received 19 February 1991)

We present a theoretical study of the influence of laser-induced continuum structure on the third-harmonic generation in atomic gases. We employ the density-matrix formalism including the spatiotemporal structure of laser pulses. The theoretical model is then applied to third-harmonic generation in sodium experiments. Extensive numerical calculations using realistic atomic parameters in combination with the parameters in actual experimental situations demonstrate the subtle interplay of various effects and pinpoint causes of possible complications. We obtain good agreement with the few existing experimental data.

PACS number(s): 32.80.-t, 42.65.Ky

I. INTRODUCTION

The scheme for laser-induced continuum structure (LICS) in its simplest form is depicted in Fig. 1(a). It requires two states (the ground and one bound excited state, $|g\rangle$ and $|a\rangle$, respectively) of a one-electron atom, and two lasers of frequencies ω_1 and ω_2 (with respective intensities I_1 and I_2). The frequencies are chosen so that $E_g + \hbar\omega_1 \simeq E_a + \hbar\omega_2$, where $E_g + \hbar\omega_1$ lies above the ionization energy. In the absence of the second laser at ω_2 , we simply have ionization. If now the second laser is present and ω_2 is fixed, while ω_1 is tuned around $E_a + \hbar\omega_2 - E_g$, under certain circumstances (depending on the states, the frequencies, and the intensities) a resonantlike peak, possibly exhibiting some asymmetry, will appear if ionization is measured as a function of ω_1 . Formal aspects of the theory of this effect have appeared in numerous papers over the past ten years [1-4]. A quantitative study of the experiment by Heller *et al.* [5] corresponding to the scheme of Fig. 1(a) has been published by Dai and Lambropoulos [6], who have shown that the complete temporal analysis [including additional couplings shown by dashed lines in Fig. 1(a)] combined with realistic atomic parameters is necessary for even a qualitative understanding. Although only two atomic states are involved in this scheme, a single rate (transition probability per unit time) involving a q parameter will usually be inadequate, if not misleading, because of the other interaction channels involved in the process. The formal similarity of this process with autoionization has also been amply discussed [1-6], hence the alternative term "autoionizinglike" often used instead of LICS.

More complicated schemes involving LICS, where at least one of the transitions requires more than one pho-

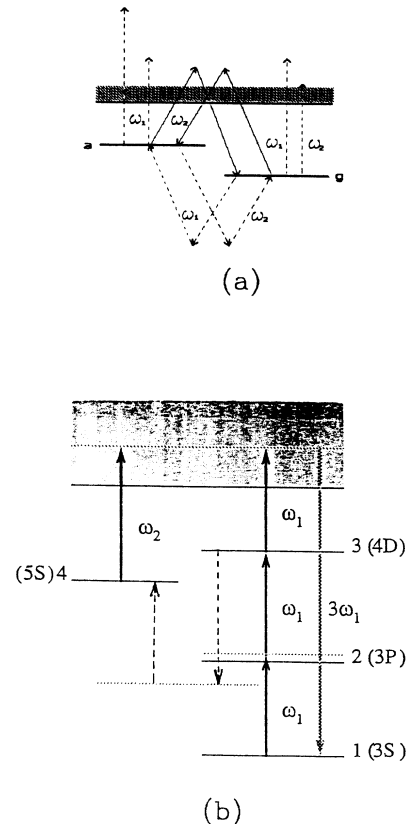


FIG. 1. (a) The simplest illustration for laser-induced continuum structure (LICS). $|g\rangle$ and $|a\rangle$ are the ground and bound excited states, respectively. (b) Energy levels of Na involved and the relevant couplings. The dashed lines represent the coupling between state 2 and 4 through virtual discrete states.

non, such as the one depicted in Fig. 1(b), poses a much more demanding theoretical problem. Not only do multiphonon transitions involve more than the two states chosen for the coupling with the two lasers, but some of these states may themselves be strongly coupled to the whole process. In that case, the relevant states must also be explicitly included in the time-dependent density-matrix analysis. Further complexity is created by the increased number of paths that participate in this case, shown by dashed lines in Fig. 1(b). The importance of such paths has been noted by Feldmann *et al.* [7] and documented quantitatively by Dai and Lambropoulos [6]. The higher intensity normally required for observations of this (multiphoton) version of LICS may itself introduce unwanted effects by emphasizing certain channels of ionization. As one consequence of significant ionization of the focal volume, there is a depletion of the number of atoms which participate in the third-harmonic generation (THG) process. Consequently, the time dependence of the overall process plays an even more decisive role on the shape, if not the very occurrence, of the structure (resonance) and practically rules out any single-rate approximations. Depending on the duration of the pulse, ionization may be complete in the central part of the focal region, which then makes integration over the spatial distribution of the lasers' intensities necessary, as is indeed the case in this work.

A further dimension of complexity is involved in the theoretical formalism of this paper. It arises from the simultaneous presence of THG which appears above a certain number density (gas pressure). Part of the question is whether THG will be affected by LICS, how much, and in what direction; will it increase or decrease? In fact, the initial motivation for investigations of THG under LICS was, and still is, the expectation that the yield of THG may thus be increased. To the best of our knowledge, the only observation of these effects, namely resonantlike structure and enhancement of THG under LICS, has been reported some years ago by Pavlov and co-workers [8,9]. The theoretical interpretation of their data relied on a transition probability (including the use of a susceptibility), which although adequate for their conditions, can neither address more general situations nor provide any clue as to the expected presence or absence of structure in THG under different conditions. Some theoretical work on the relation between THG and laser-induced continuum resonances in atomic lithium has also been published by Ritchie [10].

The problem addressed in this work combines in one context resonant and nonresonant multiphoton transitions, LICS, and THG. For relatively higher intensities and longer pulse durations, we must also deal with the spatiotemporal aspects of the interaction. As we shall see later on, certain spatial overlap considerations play a pivotal role in that case.

Even without LICS, the treatment of THG in this problem is not straightforward as it involves a two-photon resonance. That alone, would require a density-matrix analysis, as has been extensively discussed [11] in the past. The interest in two-photon resonant THG some fifteen years ago stemmed from the enhancement provid-

ed by the atomic resonance whose shift and ionization also set the ultimate limitation of that benefit [11]. In principle, LICS also provides enhancement through a resonance induced artificially by a second laser via the continuum. It has its own ultimate limitations, set mainly by the intensity of the second laser. These two resonant enhancements can in fact coexist, if ω_2 is chosen appropriately. Whether the net effect of such coexistence is more or less than the sum of its parts will depend on the circumstances created by the parameters in a given implementation.

The initial motivation for this came from the experimental results of Baldwin *et al.*, [12] whose purpose was to reproduce and extend the results of Refs. [8,9]. That, however, turned out not to be feasible under the conditions of their experiment, which employed a laser of rather long pulse duration of 25 ns. This has played a crucial role in the outcome due to the saturation of ionization resulting from such long-time exposure of the atom to the field for intensities that are necessary for LICS. We have thus chosen to center our specific calculations around parameters pertaining to that situation as well as to that of Refs. [8,9]. This has provided an interesting and valuable illustration of the constraints imposed upon intensity when the pulse is long. The resulting saturation does then necessitate integration over and sensitivity to the integration volume which has proven to be a major concern in our results.

In Sec. II we develop the formal theory incorporating all of the effects discussed above. Using this formalism, we perform calculations, some of which pertain to the data of Refs. [8,9]. Our results are discussed in Sec. III with a summary and conclusions given in Section IV. All atomic parameters entering our equations have been calculated for this purpose using single-channel quantum-defect theory with programs we have developed over the years. From the experience we have gained through the application of these techniques to a variety of problems and atoms, including sodium, we consider the accuracy of these parameters to be more than sufficient for our purposes here.

II. THEORY

The energy levels involved in our problem are shown in Fig. 1(b).

There are two lasers involved in the experiments, lasers 1 and 2. The third-harmonic signal generated by laser 1 is measured. Our goal is to calculate the third-harmonic spectrum under various experimental conditions.

In order to determine the polarization of the medium in the presence of resonances, we need to know the density-matrix elements, which can be obtained by solving the density-matrix equations of the four-level system [Fig. 1(b)] under the following Hamiltonian:

$$H = H_a + H'(t), \quad (1)$$

where H_a is the atomic Hamiltonian, $H'(t)$ is the dipole interaction of the atom with the external electric field defined by

$$H'(t) = \boldsymbol{\mu} \cdot \mathbf{E}(t), \quad (2)$$

and

$$\boldsymbol{\mu} = -e\mathbf{r}, \quad (3)$$

where e is the electron charge (negative), $\mathbf{E}(t) = E_1(t)\mathbf{e}_1 + E_2(t)\mathbf{e}_2$, with $E_1(t)$ and $E_2(t)$ being the time-dependent electric-field amplitudes for lasers 1 and 2, respectively, and \mathbf{e}_1 and \mathbf{e}_2 the unit polarization vectors of the two electric fields. When the two laser fields have the same polarization, we can simply replace \mathbf{e}_1 and \mathbf{e}_2 by \mathbf{e} , and write

$$\mathbf{E}(t) = E(t)\mathbf{e}, \quad (4)$$

where

$$E(t) = \varepsilon_1(t)e^{i\omega_1 t} + \varepsilon_1^*(t)e^{-i\omega_1 t} + \varepsilon_2(t)e^{i\omega_2 t} + \varepsilon_2^*(t)e^{-i\omega_2 t} \quad (5)$$

and $\varepsilon_j(t)$ ($j=1,2$) represents the time dependence (much slower than the exponentials) due to the pulsed character of the fields. In Eq. (5), we have not included the third-harmonic field because it is relatively weak and can be assumed not to alter the atomic system by reabsorption. We do introduce that field later [see Eqs. (26) and (34)] when we need the third-order response of the system and after we have incorporated all necessary effects due to the external fields E_1 and E_2 (such as ionization, Rabi couplings, LICS, etc.).

The equation of motion of the density matrix is

$$i\hbar \frac{\partial}{\partial t} \rho = [H, \rho], \quad (6)$$

which leads to the following set of equations for the matrix elements involving the states strongly (near-

resonantly) coupled to the fields of Eq. (5):

$$\frac{\partial}{\partial t} \rho_{ii} = -i\hbar^{-1} E(t) \left[\sum_j (\mu_{ij} \rho_{ji} - \rho_{ij} \mu_{ji}) + \sum_l (\mu_{il} \rho_{li} - \rho_{il} \mu_{li}) \right], \quad (7)$$

$$\left[\frac{\partial}{\partial t} + i\omega_{ij} \right] \rho_{ij} = -i\hbar^{-1} E(t) \left[\sum_k (\mu_{ij} \rho_{kj} - \rho_{ik} \mu_{kj}) + \sum_l (\mu_{il} \rho_{lj} - \rho_{il} \mu_{lj}) \right], \quad (8)$$

$$\left[\frac{\partial}{\partial t} + i\omega_{il} \right] \rho_{il} = -i\hbar^{-1} E(t) \left[\sum_k (\mu_{ik} \rho_{kl} - \rho_{ik} \mu_{kl}) \right], \quad (9)$$

where $i, j, k = 1, 2, 3, 4$, represent the discrete bound energy levels $3S$, $3P$, $4D$, and $5S$, respectively, with l indicating the appropriate intermediate states, bound and free.

Introducing the matrix elements σ_{ii} and $\sigma_{ij}(n, m)$ through the expansions

$$\rho_{ii} = \sigma_{ii}, \quad (10)$$

$$\rho_{ij} = \sum_{n,m} \sigma_{ij}^{(n,m)} e^{i(n\omega_1 + n\omega_2)t}, \quad (11)$$

$$\rho_{il} = \sum_{n,m} \sigma_{il}^{(n,m)} e^{i(n\omega_1 + m\omega_2)t}, \quad (12)$$

we first substitute Eq. (10) into Eq. (9), and neglecting $(\partial/\partial t)\sigma_{il}$ we obtain

$$\begin{aligned} \sigma_{il}^{(n,m)} = & - \sum_k \mu_{ik} \frac{\varepsilon_1 \sigma_{kl}^{(n-1,m)} + \varepsilon_1^* \sigma_{kl}^{(n+1,m)} + \varepsilon_2 \sigma_{kl}^{(n,m-1)} + \varepsilon_2^* \sigma_{kl}^{(n,m+1)}}{\hbar(n\omega_1 + m\omega_2 + \omega_{il})} \\ & + \sum_k \mu_{kl} \frac{\varepsilon_1 \sigma_{ik}^{(n-1,m)} + \varepsilon_1^* \sigma_{ik}^{(n+1,m)} + \varepsilon_2 \sigma_{ik}^{(n,m-1)} + \varepsilon_2^* \sigma_{ik}^{(n,m+1)}}{\hbar(n\omega_1 + m\omega_2 + \omega_{il})}. \end{aligned} \quad (13)$$

The four energy levels in our system are well separated in energy, so the coupling between σ_{il} and σ_{kl} when $i \neq k$ can be neglected. Then we can further simplify the above equation as

$$\sigma_{il}^{(n,m)} = \sum_k \mu_{kl} \frac{\varepsilon_1 \sigma_{ik}^{(n-1,m)} + \varepsilon_1^* \sigma_{ik}^{(n+1,m)} + \varepsilon_2 \sigma_{ik}^{(n,m-1)} + \varepsilon_2^* \sigma_{ij}^{(n,m+1)}}{\hbar(n\omega_1 + m\omega_2 + \omega_{il})}. \quad (14)$$

Substituting Eq. (14) together with Eqs. (10) and (11) into Eqs. (7) and (8), and keeping only the lowest-order resonant terms among the four resonantly coupled states, we arrive at the following set of equations:

$$\frac{\partial}{\partial t} \sigma_{11} = -\text{Im}(\sigma_{12}\Omega_1), \quad (15)$$

$$\frac{\partial}{\partial t} \sigma_{22} = \text{Im}(\sigma_{12}\Omega_1 - \sigma_{23}\Omega_2), \quad (16)$$

$$\left[\frac{\partial}{\partial t} + \gamma_3 \right] \sigma_{33} = \text{Im}(\sigma_{23}\Omega_2 - \sigma_{34}M_{34}\varepsilon_1\varepsilon_2^*), \quad (17)$$

$$\left[\frac{\partial}{\partial t} + \gamma_4 \right] \sigma_{44} = \text{Im}(\sigma_{34}M_{34}^*\varepsilon_1\varepsilon_2^*), \quad (18)$$

$$\begin{aligned} \left[\frac{\partial}{\partial t} + i\Delta_1 + b_1 \frac{\beta^2}{\beta^2 + \Delta_1^2} \right] \sigma_{12} \\ = -\frac{i}{2}(\sigma_{22} - \sigma_{11})\Omega_1^* + \frac{i}{2}\sigma_{13}\Omega_2, \end{aligned} \quad (19)$$

$$\left[\frac{\partial}{\partial t} + i(\Delta_1 + \Delta_2) + \frac{\gamma_3}{2} + 4b_1 \frac{\beta^2}{\beta^2 + (\Delta_1 + \Delta_2)^2} \right] \sigma_{13} \\ = -\frac{i}{2}(\sigma_{23}\Omega_1^* - \sigma_{12}\Omega_2^* - \sigma_{14}M_{34}\varepsilon_1\varepsilon_2^*), \quad (20)$$

$$\left[\frac{\partial}{\partial t} + i \left(\frac{3(\Delta_1 + \Delta_2)}{2} - \Delta_3 \right) + \frac{\gamma_4}{2} \right. \\ \left. + (9b_1 + b_2) \frac{\beta^2}{\beta^2 + [3(\Delta_1 + \Delta_2)/2 - \Delta_3]^2} \right] \sigma_{14} \\ = -\frac{i}{2}(\sigma_{24}\Omega_1^* - \sigma_{13}M_{34}\varepsilon_1^*\varepsilon_2), \quad (21)$$

$$\left[\frac{\partial}{\partial t} + i\Delta_2 + \frac{\gamma_3}{2} + b_1 \frac{\beta^2}{\beta^2 + \Delta_2^2} \right] \sigma_{23} \\ = -\frac{i}{2}(\sigma_{33} - \sigma_{22})\Omega_2^* - \frac{i}{2}(\sigma_{13}\Omega_1 - \sigma_{24}M_{34}\varepsilon_1\varepsilon_2^*), \quad (22)$$

$$\left[\frac{\partial}{\partial t} + i \left(\frac{\Delta_1 + 3\Delta_2}{2} - \Delta_3 \right) + \frac{\gamma_4}{2} \right. \\ \left. + (4b_1 + b_2) \frac{\beta^2}{\beta^2 + [(\Delta_1 + 3\Delta_2)/2 - \Delta_3]^2} \right] \sigma_{24} \\ = -\frac{i}{2}(\sigma_{14}\Omega_1 + \sigma_{34}\Omega_2^* - \sigma_{23}M_{34}\varepsilon_1^*\varepsilon_2), \quad (23)$$

$$\left[\frac{\partial}{\partial t} + i \left(\frac{\Delta_1 + \Delta_2}{2} - \Delta_3 \right) + \frac{\gamma_3 + \gamma_4}{2} \right. \\ \left. + (b_1 + b_2) \frac{\beta^2}{\beta^2 + [(\Delta_1 + \Delta_2)/2 - \Delta_3]^2} \right] \sigma_{34} \\ = -\frac{i}{2}(\sigma_{44}M_{34}^*\varepsilon_1^*\varepsilon_2 - \sigma_{33}M_{34}\varepsilon_1^*\varepsilon_2) - \frac{i}{2}\sigma_{24}\Omega_2^*, \quad (24)$$

where $\Omega_1 = 2\hbar^{-1}\mu_{12}\varepsilon_1$ is the Rabi frequency between 3S and 3P, $\Omega_2 = 2\hbar^{-1}\mu_{23}\varepsilon_2$ is the Rabi frequency between 3P and 4D, and $\text{Re}(M_{34}) = 2\hbar^{-2}[\sum_l \mu_{3l}\mu_{l4}/(\bar{\omega}_{3l} - \omega_2) + \text{P} \int d\omega_c \mu_{3c}\mu_{c4}/(\bar{\omega}_{3c} + \omega_1)]$ is the real part of the effective two-photon dipole moment between 4D and 5S, including the coupling through the continuum as well as

through (virtual) discrete states, with $\hbar\bar{\omega}_{3l}$ and $\hbar\bar{\omega}_{3c}$ being the energy differences between 4D and the bound and free intermediate states, respectively. $\text{Im}(M_{34}) = 2\hbar^{-2}(2\pi\mu_{3c}\mu_{c4})|_{E_c=E_3+\hbar\omega_1}$ is the imaginary part of the two-photon effective dipole moment between 4D and 5S, resulting from the resonant coupling through the continuum. $\Delta_1 = \omega_1 - \bar{\omega}_{21}$ is the detuning of ω_1 from the resonance between 3S and 3P, with $\bar{\omega}_{21}$ being the resonance between 3S and 3P. $\Delta_2 = \omega_1 - \bar{\omega}_{32}$ is the detuning of ω_1 from the resonance between 3P and 4D, with $\bar{\omega}_{32}$ being the resonance between 3P and 4D. $\Delta_3 = \omega_2 - \bar{\omega}_{c4}|_{E_c=E_3+\hbar\omega_1}$ is the detuning of ω_2 from the resonance between 5S and the continuum state which lies at $3\omega_1$ above the 3S state. $\gamma_1 = 2\hbar^{-6}(2\pi)(|\varepsilon_2|^6|\mu_{1c}|_{E_c=E_1+3\hbar\omega_2}^2)$ is the three-phonon ionization width of 3S by the absorption of $3\omega_2$ photons. $\gamma_3 = 2\hbar^{-2}(2\pi)(|\varepsilon_1|^2|\mu_{3c}|_{E_c=E_3+\hbar\omega_1}^2 + |\varepsilon_2|^2|\mu_{3c'}|_{E_c=E_3+\hbar\omega_2}^2)$ is the sum of the ionization widths of 4D, induced by ω_1 and ω_2 , separately. $\gamma_4 = 2\hbar^{-2}(2\pi)(|\varepsilon_1|^2|\mu_{4c}|_{E_c=E_4+\hbar\omega_1}^2 + |\varepsilon_2|^2|\mu_{4c'}|_{E_c=E_4+\hbar\omega_2}^2)$ is the sum of the ionization widths of 5S, and also induced by ω_1 and ω_2 , separately.

The laser bandwidths are also included with $2b_1$ and $2b_2$ representing the full width at half maximum of the two lasers respectively. As has been discussed in Ref. [13], a cutoff frequency β needs to be included to eliminate the consequences introduced by the long wings of the Lorentzian line shape, such as unphysical incoherent populations of the intermediate states far from resonance.

All levels of the atomic system undergo ac Stark shifts under the influence of both external fields. The four levels included in the density matrix do not contribute to such shifts because their effect on each other is included in the density-matrix equations. After having ascertained (through calculations) that the ac Stark shifts due to all other atomic levels are negligible, we have omitted them from the equations.

The solution of Eqs. (15)–(24) under prescribed laser pulses provides the state of the atomic system as a function of time.

The generation of the third-harmonic wave is due to the nonlinear polarizability of the atomic medium. In the density matrix formalism, the polarizability per atom is defined by

$$P(z, t) \equiv \text{Tr}[\rho(z, t)\mu] \\ \equiv \sum_i \left[\sum_l (\mu_{il}\rho_{li} + \mu_{li}\rho_{il}) + \sum_j \mu_{ji}\rho_{ij} \right]. \quad (25)$$

Had we included the third harmonic field $E_3(t) = \varepsilon_3 e^{i3\omega_1 t}$ in Eqs. (7) and (8), instead of Eq. (13), we would have had

$$\sigma_{il}^{(n,m)} = \sum_k \mu_{kl} \frac{\varepsilon_1 \sigma_{ik}^{(n-1,m)} + \varepsilon_1^* \sigma_{ik}^{(n+1,m)} + \varepsilon_2 \sigma_{ik}^{(n,m-1)} + \varepsilon_2^* \sigma_{ik}^{(n,m+1)} + \varepsilon_3 \sigma_{ik}^{(n-3,m)} + \varepsilon_3^* \sigma_{ik}^{(n+3,m)}}{\hbar(n\omega_1 + m\omega_2 + \omega_{il})}. \quad (26)$$

From classical electrodynamics we have the following definition for the linear polarizability due to E_1 :

$$P_{\omega_1}(z, t) \equiv [\chi'(\omega_1) + i\chi''(\omega_1)]\epsilon_1 e^{i(\omega_1 t - k_1 z)} + \text{c. c.} \quad (27)$$

where $\chi'(\omega_1)$ and $\chi''(\omega_1)$ are the real and imaginary parts of the linear susceptibility of the medium at ω_1 . From Eq. (25), we can express the susceptibility in terms of the quantum-mechanical state of the atomic system as

$$\begin{aligned} \chi'(\omega_1) = & \sum_i \alpha'_i(\omega_1) \sigma_{ii}^{(0,0)} + (\mu_{21} \text{Re} \sigma_{12}^{(1,0)} + \mu_{32} \text{Re} \sigma_{23}^{(1,0)}) / \epsilon_1 \\ & + \hbar^{-1} \text{Re} \left[\mu_{43}(\omega_1) \sigma_{34}^{(1,-1)} \frac{\epsilon_2}{\epsilon_1} \right], \end{aligned} \quad (28)$$

where

$$\alpha'_i(\omega_1) = \sum_l \left[\frac{|\mu_{il}|^2}{\omega_{il} + \omega_1} + \frac{|\mu_{il}|^2}{\omega_{il} - \omega_1} \right] \quad (29)$$

and

$$\mu_{43}(\omega_1) = \sum_l \frac{\mu_{4l} \mu_{l3}}{\omega_{4l} - \omega_1} + \sum_l \frac{\mu_{4l} \mu_{l3}}{\omega_{3l} + \omega_1}. \quad (30)$$

From Maxwell's equations, we have

$$E_1 = \epsilon_1(z, t) e^{i(\omega_1 t - k_1 z)}, \quad (31)$$

where

$$k_1 = \frac{\omega_1}{c} \left[1 + \frac{N\chi'(\omega_1)}{2\epsilon_0} \right] = \frac{\omega_1}{c} n_{\omega_1}, \quad (32)$$

N being the density of atoms. Similarly, we can obtain the linear part of the response of the medium to the third-harmonic signal, expressed as

$$P_{3\omega_1}^L(z, t) = \sum_i \alpha'_i(3\omega_1) \sigma_{ii} E_3(z, t), \quad (33)$$

where

$$E_3(z, t) = \epsilon_3(z, t) e^{i(3\omega_1 t - k_3 z)} \quad (34)$$

and

$$k_3 = \frac{3\omega_1}{c} \left[1 + \frac{N\chi'(3\omega_1)}{2\epsilon_0} \right] = \frac{3\omega_1}{c} n_{3\omega_1}. \quad (35)$$

We also need the nonlinear part of the polarizability given by [12]

$$N_{3\omega_1} = \frac{3\omega_1 N^2 L^2}{4\hbar^3 c^2 \epsilon_0^2} \int \left[\frac{\sin(\Delta k L / 2)}{\Delta k L / 2} \right]^2 \left| \mu_{31}(3\omega_1) \sigma_{13}^{(2,0)} + \mu_{41}(3\omega_1) \sigma_{14}^{(3,-1)} \left[\frac{I_2}{I_1} \right]^{1/2} \right|^2 I_1(t) dt. \quad (41)$$

Taking into account the fact that the laser pulse is a function of both location and time, we solve the density-matrix equations numerically with a pulse which has the time-dependence shown below, and integrate spatially in order to account for the effect of saturation due to the strong laser intensities and the pulse duration.

The form of the intensity distribution of the laser pulse

$$\begin{aligned} P_{3\omega_1}^{\text{NL}} = & \hbar^{-1} [\mu_{31}(3\omega_1) \sigma_{13}^{(2,0)} \epsilon_1 + \mu_{41}(3\omega_1) \sigma_{14}^{(3,-1)} \epsilon_2] \\ & \times e^{i(3\omega_1 t - 3k_1 z)} + \text{c. c.}, \end{aligned} \quad (36)$$

where

$$\mu_{31}(3\omega_1) = \sum_l \frac{\mu_{3l} \mu_{l1}}{\omega_{3l} - 3\omega_1} + \sum_l \frac{\mu_{3l} \mu_{l1}}{\omega_{l1} + 3\omega_1} \quad (37)$$

and

$$\mu_{41}(3\omega_1) = \sum_l \frac{\mu_{4l} \mu_{l1}}{\omega_{4l} - 3\omega_1} + \sum_l \frac{\mu_{4l} \mu_{l1}}{\omega_{l1} + 3\omega_1}. \quad (38)$$

Substituting Eqs. (33) and (37) into Maxwell's equations, and keeping only the first-order derivatives, we obtain the wave equation for the third-harmonic field:

$$\begin{aligned} \frac{\partial}{\partial z} \epsilon_3 + \frac{n_{3\omega_1}}{c} \frac{\partial}{\partial t} \epsilon_3(z, t) \\ = i \frac{3\omega_1 N}{2\epsilon_0 c \hbar} [\mu_{31}(3\omega_1) \sigma_{13}^{(2,0)}(0, t) \epsilon_1(z, t) \\ + \mu_{41}(3\omega_1) \sigma_{14}^{(3,-1)}(z, t) \epsilon_2(z, t)] e^{-i\Delta k z}, \end{aligned} \quad (39)$$

where $\Delta k = 3k_1 - k_3$.

When the laser pulse duration is much longer than the transit time through the cell, which is the case here, the time derivative in the wave equation can be neglected. Also taking advantage of the fact that the effective length of the sodium cell is often relatively small, we can avoid the complicated consideration of the phase matching in a focused beam. If we consider the phase mismatch Δk , the slowly varying part of the laser field E , and the density-matrix elements σ as being independent of z , we obtain

$$\begin{aligned} \epsilon_3(L, t) = i \frac{3\omega_1 N}{2\epsilon_0 c \hbar} [\mu_{31}(3\omega_1) \sigma_{13}^{(2,0)} \epsilon_1(t) \\ + \mu_{41}(3\omega_1) \sigma_{14}^{(3,-1)} \epsilon_2(t)] \frac{e^{-i\Delta k L} - 1}{(-i\Delta k)}. \end{aligned} \quad (40)$$

where L is the length of the sodium cell.

Thus the number of third-harmonic photons per pulse unit area can be written as

is here taken as

$$\begin{aligned} I(r, z, t) = \frac{I_0 \text{sech}^2(1.76t/\tau)}{1 + A \lambda^2 z^2 / \phi^2 r_0^4} \\ \times \exp \left[-\frac{2r^2}{r_0^2 (1 + A \lambda^2 z^2 / \phi^2 r_0^4)} \right], \end{aligned} \quad (42)$$

which is the usual expression representing focused beams. More details on the definition of the constants appearing in Eq. (42) can be found, for example, in Ref. [14].

To calculate the spatial average, we need to perform the integration with respect to the spatial variables. As we have pointed out earlier, when the effective length of the sodium cell is relatively small, we can also disregard the z dependence of the laser intensity. The intensity distribution equation above can then be simplified as

$$I = I_M \exp[-2(r/r_0)^2], \quad (43)$$

in which case we have

$$\bar{N}_{3\omega_1} = \frac{\int_0^{r_{\max}} N_{3\omega_1}(r) r dr}{\int_0^{r_{\max}} r dr} = \frac{\int_{I_{\min}}^{I_M} N_{3\omega_1}(I) dI / I}{\int_{I_{\min}}^{I_M} dI / I}, \quad (44)$$

I_{\min} being the value of the intensity at $r = r_{\max}$.

III. CALCULATIONS AND RESULTS

A. Single-laser case

We choose the following set of parameters: $I_1 = I_2 = 2.2 \times 10^{10}$ W/cm², $\tau = 25$ ns, vapor length $L \sim 8$ cm, and density of atoms $N = 10^{22}$ /m³. In the single-laser case, we have $I_2 = 0$, and the third-harmonic signal is examined as a function of the detuning from the two-photon resonance with $4D$. In an experiment by Baldwin *et al.* [12], a peak has been observed at resonance, as well as a sharp dip at the center of the peak.

Figure 2 here shows a series of calculated third-harmonic spectra under different laser intensities. It can be seen that the widths of the spectra depend very sensitively on the laser intensity. Moreover, the calculations indicate that the ionization becomes saturated at intensities above 10^8 W/cm². As a result, contributions from different spatial regions in the focal volume would be expected to play a very important role.

Figure 3 shows one example of the resulting third-harmonic spectrum obtained after integration over the focal volume. The dip near the center of the spectrum results from the competition between the ionization and the THG. As a matter of fact, this dip corresponds to a peak in the ionization spectrum. It appears only when the ionization peak is saturated.

B. Two-laser experiments

For the case in which the first laser is fixed at the two-photon resonance with the $4D$ level, calculated results of the third-harmonic spectra versus the detuning of the second laser at different intensities are shown in Fig. 4. First we note the small peak near the resonance, which is the result of LICS. There is, however, a broad peak even at intensities as low as $I_1 = I_2 = 5 \times 10^7$ W/cm² [Fig. 4(d)]. At lower intensities ($I_1 = I_2 = 10^7$ W/cm²) the broad peak disappears. The small LICS peak is so small and narrow that it could easily be buried in the fluctuations of an experimental background. The broad feature, however, should readily show in an experiment since it is

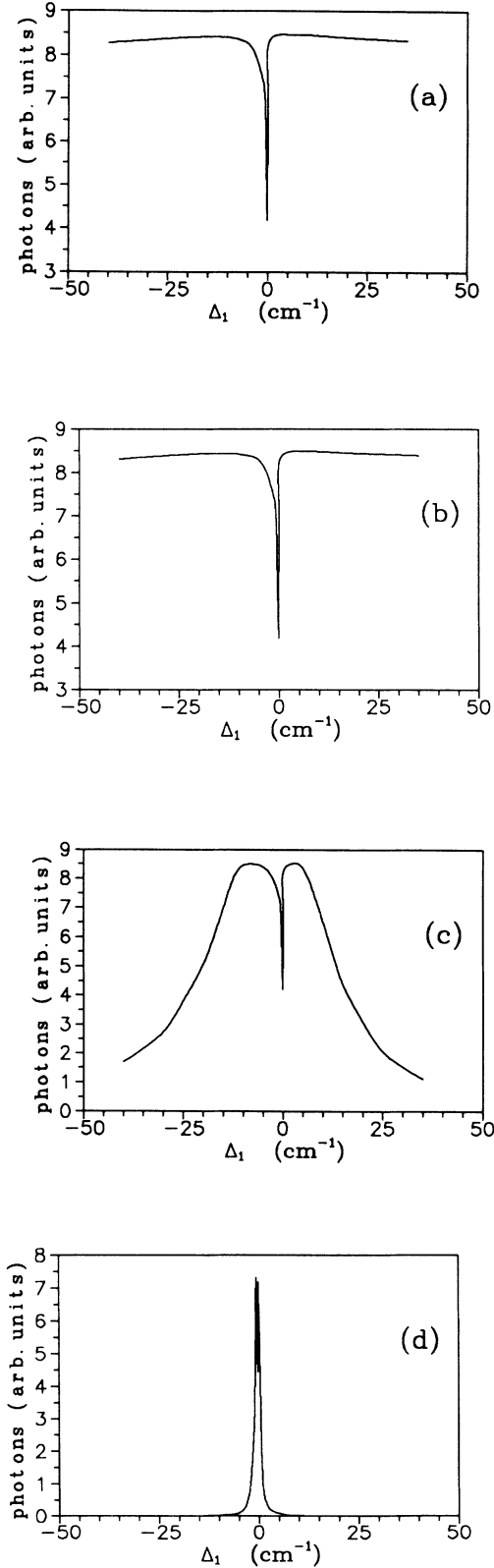


FIG. 2. Calculated third-harmonic spectrum for single-laser experiment with different laser intensities. $\Delta_1 = 0$ corresponds to $2\omega_1 = E_{4d}$. (a) $I_1 = 2.2 \times 10^{10}$ W/cm². (b) $I_1 = 5.0 \times 10^9$ W/cm². (c) $I_1 = 1.0 \times 10^9$ W/cm². (d) $I_1 = 1.0 \times 10^8$ W/cm². Arbitrary units are used for the number of the third-harmonic photons.

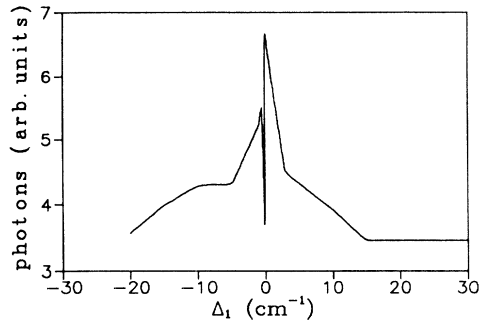


FIG. 3. One example of the resulting third-harmonic spectrum obtained after the spatial average in the r -direction. Arbitrary units are used for the number of the third-harmonic photons.

still prominent even after spatial integration.

But considering that we have calculated the spectra assuming that both lasers have a complete spatiotemporal overlap, we consider the possibility that our calculation may differ from a real experimental situation if the two lasers do not have such a complete overlap. To test the sensitivity of the broad feature to the spatial overlap, we have calculated the third-harmonic spectrum for different combinations of intensities of the two lasers, as shown in Fig. 5. Clearly, the broad peak disappears even at rather high intensities, as the second laser intensity is reduced. Through further investigation, we have found that this broad peak is most pronounced when the second laser intensity is so strong that the two-photon Rabi frequency between $4D$ and $5S$ is equal to the one-photon Rabi frequency between $3P$ and $4D$. When this is the case, i.e.,

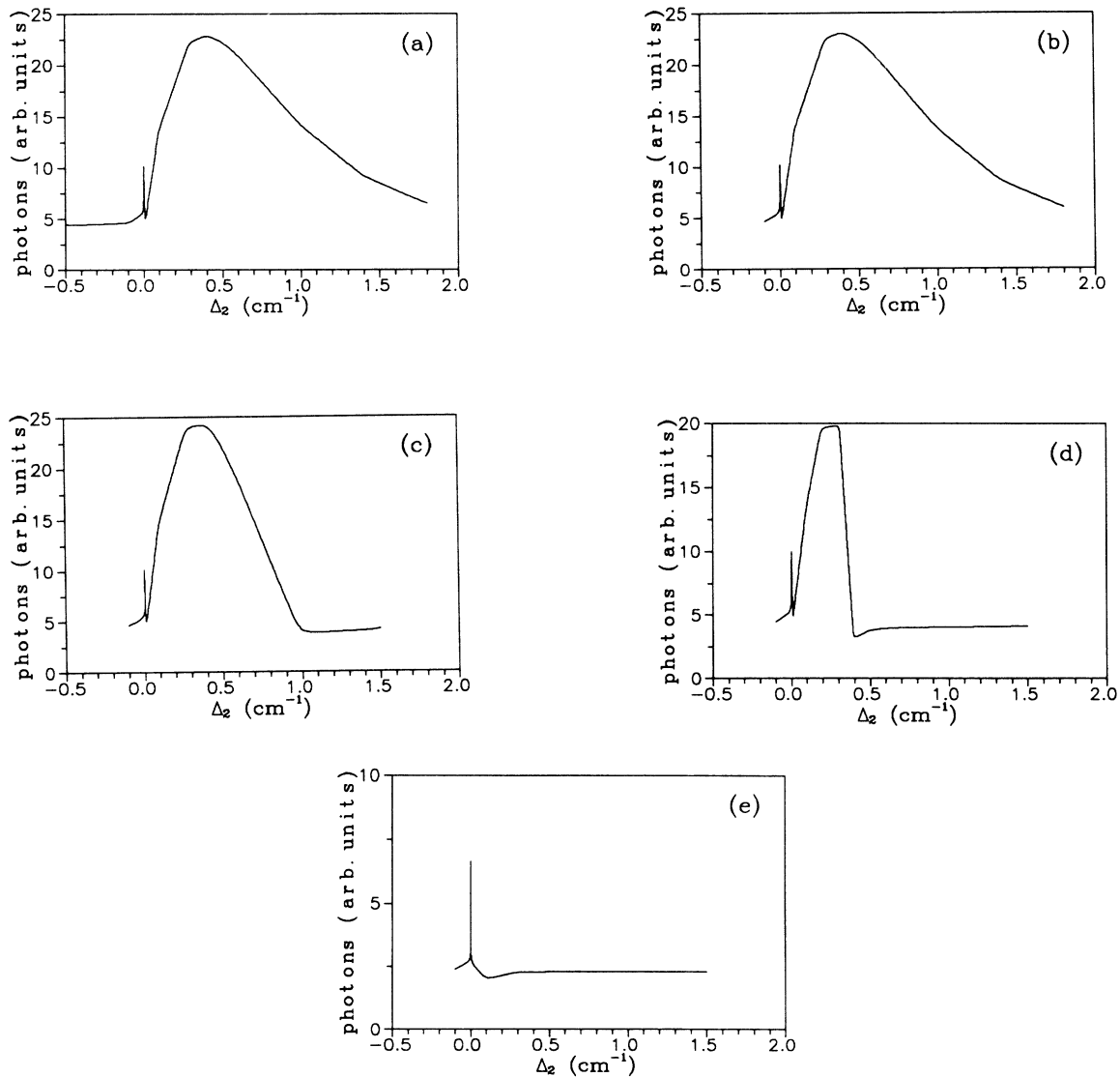


FIG. 4. Calculated third-harmonic spectrum versus the detuning of the second laser for two-laser experiment at different intensities. (a) $I_1 = I_2 = 2.2 \times 10^{10} \text{ W/cm}^2$. (b) $I_1 = I_2 = 1.0 \times 10^9 \text{ W/cm}^2$. (c) $I_1 = I_2 = 1.0 \times 10^8 \text{ W/cm}^2$. (d) $I_1 = I_2 = 5.0 \times 10^7 \text{ W/cm}^2$. (e) $I_1 = I_2 = 1.0 \times 10^7 \text{ W/cm}^2$. Arbitrary units are used for the number of third-harmonic photons.

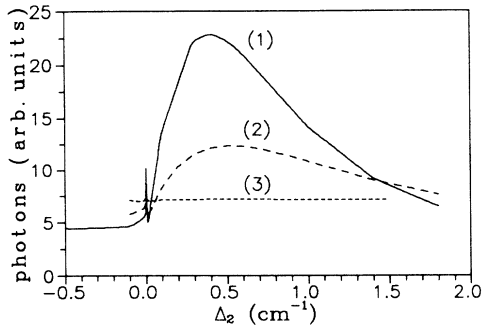


FIG. 5. Results of third-harmonic spectrum with different combinations of intensities. Curve (1) taken from Fig. 4(a). Curve (2) is calculated at $I_1 = 2.2 \times 10^{10}$ W/cm², $I_2 = 1.0 \times 10^{10}$ W/cm². Curve (3) is calculated at $I_1 = 2.2 \times 10^{10}$ W/cm², $I_2 = 1.0 \times 10^9$ W/cm².

the two Rabi frequencies are equal, the coherence in the excitation of these three energy levels is the strongest. Thus the physical origin of this double-peak structure can be attributed to the ac Stark splitting of the $4D$ state due to its two-photon coupling to the $3S$. To test this interpretation, we have calculated a series of line shapes for different intensities of the first laser and we present the results in Figs. 6(a)–6(c). For reasons of economy in computation time, we have performed these calculations for considerably shorter pulse durations (0.1 ns). The actual pulse duration should not matter here because what we need is to test the dependence of the splitting on the laser intensity. Since we are arguing that the splitting is a result of a two-photon Rabi frequency (which is proportional to the square of the field amplitude), the distance between the two peaks should be proportional to the intensity of the first laser, which is indeed the case in Fig. 6(a)–6(c), thus confirming the origin of the structure.

In Fig. 7, we show the third-harmonic spectrum versus the detuning of the first laser calculated when a second laser at frequency $\omega_{20}(\hbar\omega_{20} + E_{5s} = \hbar\omega_{10} + E_{4d} = 3\hbar\omega_{10} + E_{3s})$ is introduced. It is obvious that this second laser adds new features to the third harmonic spectrum shown in Fig. 2. But these new features also disappear when the second laser intensity becomes insufficient. Shown in Fig. 8 is the spectrum calculated at different intensities of the second laser. The new features disappear as the intensity of the second laser decreases, as must be the case for structure due to LICS.

Finally, in order to test our formalism and atomic parameters, we turn to the experimental result published by Pavlov *et al.* [8] and Dimov *et al.* [9]. The pulse duration of both lasers in Refs. [8,9] was about 2 ns, while their intensity was 10^9 W/cm², and their bandwidths about 0.1 cm⁻¹.

Figure 9 shows the result calculated for the conditions of the experiment in Refs. [8,9]. The calculations reproduce a similar degree of enhancement of the LICS over the continuum (approximately a factor of 18 in the experiment). The width of the spectrum is also comparable (~ 0.5 cm⁻¹). The asymmetry is somewhat more visible than that in the experiment. Considering that the experi-

mental data must have had some error bars and the possible background noise, our calculation compares fairly well with the experimental line shape (Fig. 3 of Ref. [8] or Fig. 4 of Ref. [9]).

Finally, it should be reemphasized that ionization saturation was not present in the experiment in Refs. [8,9] due to the relatively short pulse duration. Hence the spatial effects, which are shown to be such a strong factor in determining the spectrum in Figs. 3 and 5 for a much longer pulse (25 ns), were much less important in that experiment. This makes the data less sensitive to the details of beam spatial overlap, which facilitates the theoretical interpretation and is also responsible for the marked LICS enhancement.

IV. CONCLUDING REMARKS

In this paper, we have developed a thorough time-dependent density-matrix theory for third-harmonic gen-

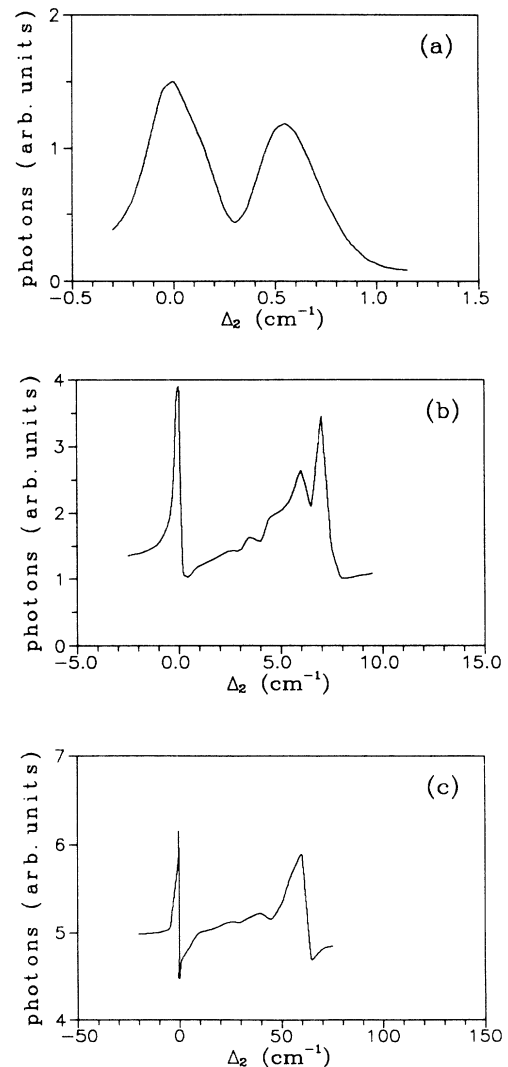


FIG. 6. Calculated third-harmonic spectrum for two-laser experiment with laser pulse duration of 0.1 ns, $I_2 = 1.0 \times 10^9$ W/cm². (a) $I_1 = 1.0 \times 10^8$ W/cm². (b) $I_1 = 1.0 \times 10^9$ W/cm². (c) $I_1 = 1.0 \times 10^{10}$ W/cm². Arbitrary units are used for the number of the third-harmonic photons.

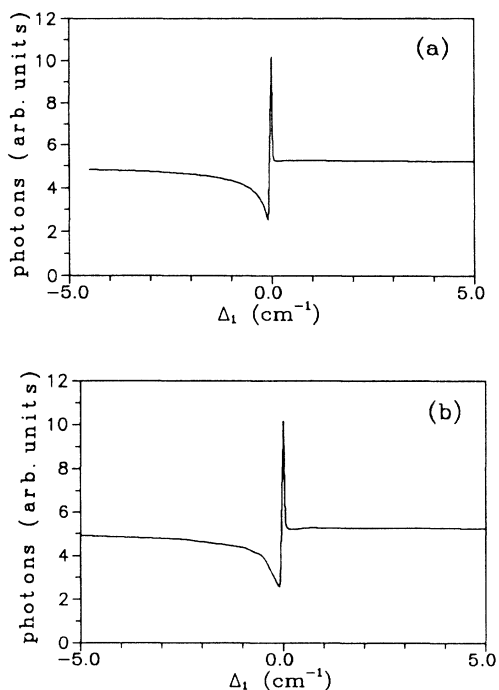


FIG. 7. Calculated third-harmonic spectrum versus the detuning of the first laser for two-laser experiment. The second laser frequency is fixed at ω_{20} ($\hbar\omega_{20} + E_{5s} = \hbar\omega_{10} + E_{4d} = 3\hbar\omega_{10} + E_{3s}$). (a) $I_1 = I_2 = 2.2 \times 10^{10}$ W/cm². (b) $I_1 = I_2 = 1.0 \times 10^9$ W/cm². Arbitrary units are used for the number of the third-harmonic photons.

eration in sodium gas in the presence of laser-induced continuum structure. We have then applied the theory to quantitative calculations using single-channel quantum-defect theory for the evaluation of atomic parameters, such as Rabi frequencies and photoionization widths. In the numerical calculations, we have made every effort to simulate real experimental conditions, such as spatiotemporal aspects of the laser pulses and have evaluated their role in shaping the third-harmonic generation spectra.

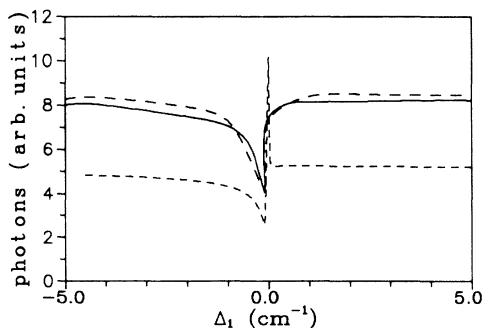


FIG. 8. The solid curve is the third-harmonic spectrum versus the detuning of laser one calculated at $I_1 = 2.2 \times 10^{10}$ W/cm², $I_2 = 1.0 \times 10^9$ W/cm². The dashed curve with a sharp peak near the center is Fig. 7(a), $I_1 = I_2 = 2.2 \times 10^{10}$ W/cm². The dashed curve on the top is Fig. 2(a), $I_1 = 2.2 \times 10^{10}$ W/cm². Arbitrary units are used for the number of the third-harmonic photons.

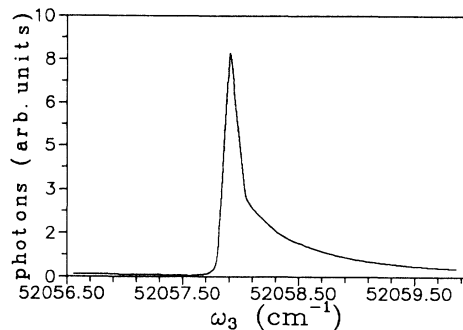


FIG. 9. Calculated third-harmonic spectrum for two-laser experiment. $I_1 = I_2 = 1.0 \times 10^9$ W/cm², $\tau_1 = \tau_2 = 2.0$ ns, $2b_1 = 2b_2 = 0.1$ cm⁻¹, and $\beta = 1.0$ cm⁻¹. $\lambda_2 = 530$ nm. Arbitrary units are used for the number of the third-harmonic photons.

Our theory and calculations show that, due to the possibility of ionization saturation, high laser intensities do not always enhance the third-harmonic generation, and that the laser-induced structure in the continuum is very sensitive to the relative intensities of the two lasers. Furthermore, experimental investigations would be very useful in clarifying the role of laser induced continuum structure in nonlinear interactions of atoms with strong radiation fields.

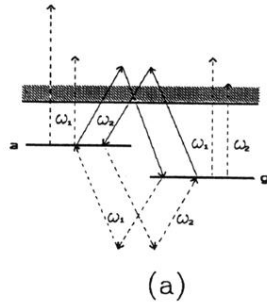
It should be evident from our analysis of the various effects entering these phenomena that large intensity is not necessarily useful. Large must of course be evaluated in the context of the pulse duration because the saturation (due to the inevitable ionization) increases with time as well as intensity. Owing to the nonlinear nature of the processes, one does not have simple rules that determine the behavior in terms of, say, the product of duration and intensity. We know, on the other hand, that a minimum of intensity is necessary, if observable LICS is to develop; this means that delicate balances between conflicting requirements determine the observability of these effects. A quantitative analysis, such as the one undertaken here, will thus be necessary for the reliable prediction and/or interpretation of experimental results.

We hope that we have demonstrated the richness and subtlety of the many nonlinear processes at play in studies of LICS. A further most interesting dimension of variety should be expected when the continuum already contains structure due to intra-atomic interactions, as is the case in more than one-electron atoms. We expect to report soon on studies of LICS combined with doubly excited autoionizing states in alkaline-earth atoms.

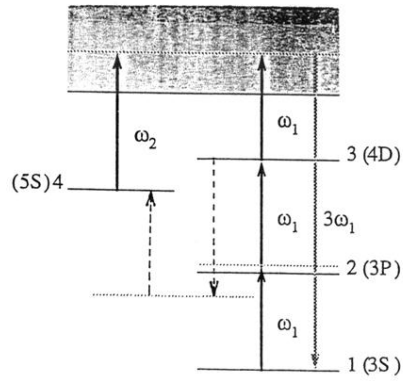
ACKNOWLEDGMENTS

We are grateful to Dr. Baldwin, Dr. Chapple, and Dr. Bachor for providing the impetus and for numerous communications during the course of this work. We also gratefully acknowledge much valuable input from discussions with Dr. Xian Tang. This work has been supported by the National Science Foundation under Grant No. PHY-9013434 and by the U.S. Department of Energy under Grant No. DE-FG03-87ER60504.

- [1] Yu. I. Geller and A. K. Popov, *Zh. Eksp. Teor. Fiz.* **78**, 506 (1980) [*Sov. Phys.—JETP* **51**, 255 (1980)].
- [2] P. E. Coleman, P. L. Knight, and K. Burnett, *Opt. Commun.* **42**, 171 (1982).
- [3] X. Tang, Anne L'Huillier, and P. Lambropoulos, *Phys. Rev. Lett.* **62**, 111 (1989); for a related experiment, see M. H. R. Hutchinson and K. M. M. Ness, *Phys. Rev. Lett.* **60**, 105 (1988).
- [4] P. L. Knight, M. A. Lauder, and B. J. Dalton, *Phys. Rep.* **190**, 1 (1990).
- [5] Yu. I. Heller, V. F. Lukinykh, A. K. Popov, and V. V. Slabko, *Phys. Lett.* **82A**, 4 (1981).
- [6] Bo-nian Dai and P. Lambropoulos, *Phys. Rev. A* **36**, 5205 (1987).
- [7] D. Feldmann, G. Otto, D. Petring, and K. H. Welge, *J. Phys. B* **19**, 269 (1986).
- [8] L. I. Pavlov, S. S. Dimov, D. I. Metchkov, G. M. Mileva, and K. V. Stamenov, *Phys. Lett.* **89A**, 441 (1982).
- [9] S. S. Dimov, L. I. Pavlov, K. V. Stamenov, Yu. I. Heller, and A. K. Popov, *Appl. Phys. B* **30**, 35 (1983).
- [10] Burke Ritchie, *Phys. Rev. A* **31**, 823 (1985).
- [11] A. T. Georges, P. Lambropoulos, and J. H. Marburger, *Phys. Rev. A* **15**, 300 (1977), and references therein.
- [12] K. G. H. Baldwin, P. B. Chapple, H.-A. Bachor, Jian Zhang, and P. Lambropoulos (unpublished); also P. B. Chapple, Ph.D. thesis, Australian National University, 1988 (unpublished).
- [13] P. Zoller and P. Lambropoulos, *J. Phys. B* **12**, L547 (1979).
- [14] O. L. Landen, M. D. Perry, and E. M. Campbell, *Phys. Rev. Lett.* **59**, 2558 (1987).



(a)



(b)

FIG. 1. (a) The simplest illustration for laser-induced continuum structure (LICS). $|g\rangle$ and $|a\rangle$ are the ground and bound excited states, respectively. (b) Energy levels of Na involved and the relevant couplings. The dashed lines represent the coupling between state 2 and 4 through virtual discrete states.